J Solid State Electrochem
DOI 10.1007/s10008-012-1965-3

REVIEW

# The electrochemistry of nanostructured Ni–W alloys

**M. P. Quiroga Argañaraz · S. B. Ribotta · M. E. Folquer · G. Benítez · A. Rubert · L. M. Gassa · M. E. Vela · R. C. Salvarezza**

Received: 27 September 2012 / Revised: 21 November 2012 / Accepted: 26 November 2012


**Abstract** This work reports on the features that Ni–W nanostructured alloys, electrodeposited on carbon steel by different current pulse programs, may present depending on their surface morphology and surface composition. The Ni–W nanostructured coating, with a cauliflower structure, lack of fragility, and high $WO_3$/W surface composition ratio, is a stable electrode to catalyze hydrogen evolution reaction, exceeding bulk and electrodeposited Ni catalytic activity. Also, the nanostructured alloys must have a low $WO_3$/W surface composition ratio for Ni and its oxides to provide protection and improve corrosion resistance in sulfate media.

**Keywords** Pulse electrodeposition · Ni–W alloys · Nanostructured materials · XPS · Corrosion resistance · Hydrogen evolution reaction

## Introduction

Electrodeposition alloy coating production is interesting because its processing parameters are easy to control. In this sense, research on plated nickel–tungsten (Ni–W) alloys has increased as they exhibit optimum hardness and good corrosion and wear resistance. These improved characteristics, together with good ductility and high thermal stability, can be achieved through nanostructured electrodeposits [1–14]. However, the main features of these coatings are very sensitive to the selected experimental conditions. The strong dependence of the electrodeposition parameters (bath composition, pH, temperature, and current density) on the Ni–W alloy composition, structure, surface morphology, grain size, and even the presence or not of microcracks has already been demonstrated [2, 3, 7, 11, 15–21]. Another aspect to be taken into account is whether the deposition was carried out with direct [2, 5, 8, 10, 14, 16, 17, 21–25] or pulsed currents [7, 9, 11, 13, 18, 25, 26] since they determine the different results related to properties and characteristics of the electrodeposited alloys.

Regarding Ni–W alloy corrosion behavior, previous scientific works carried out in NaCl [4, 6, 8, 10–14, 21, 25] and $H_2SO_4$ [6, 24] solutions provide different interpretations that reflect its complexity.

Prediction of the electrochemical behavior of nanocrystalline materials from the properties of their coarse-grained and amorphous analogs is not straightforward because of the differences in their surface characteristics. The interdependence of the parameters mentioned before is thus confirmed [27].

In our previous work, we selected a neutral electrolyte containing sulfate anions to demonstrate that Ni–W coatings protected the carbon steel substrate from pitting [11, 28]. We interpreted the electrochemical results taking into account the contribution of the coating components [11].

Our research is currently focused on studying how surface morphology and composition of current pulse formed Ni–W alloys (particularly concentration ratios between metallic components and their oxides) affect corrosion resistance and hydrogen evolution reaction (HER) catalysis in the aforementioned electrolyte. Bulk and electrodeposited Ni are also presented for the sake of comparison.

## Experimental

Nanocrystalline Ni–W and Ni coatings were deposited on carbon steel (SAE 1020) sheets (area=1 $cm^2$) previously

M. P. Quiroga Argañaraz · S. B. Ribotta · M. E. Folquer (✉)
Instituto de Química Física, Facultad de Bioquímica, Química y Farmacia, INQUINOA-CONICET, Universidad Nacional de Tucumán, Ayacucho 471 (4000) San Miguel de Tucumán, Argentina
e-mail: mefolquer@fbqf.unt.edu.ar

G. Benítez · A. Rubert · L. M. Gassa · M. E. Vela · R. C. Salvarezza
Instituto de Investigaciones Fisicoquímicas Teóricas y Aplicadas (INIFTA) Facultad de Ciencias Exactas, Universidad Nacional de La Plata–CONICET, Suc. 4, CC 16, La Plata, Argentina

Published online: 13 December 2012

polished with sandpaper, decreasing in grit size from 80 to 2500, followed by 0.3 μm alumina powder and finally rinsed with twice-distilled water.

The electrodeposited coatings were obtained galvanostatically by pulse electroplating using a Solartron system 12508W, which includes a frequency response analyzer 1250 and an electrochemical interface 1287. The pulse scheme consisted of an "on" time ($\tau_{on}$) during which a cathodic current of 70 mA $cm^{-2}$ was applied and an "off" time ($\tau_{off}$) during which a zero current was applied, where $\tau=\tau_{on}=\tau_{off}$, with $5\times10^{-3}$ s≤τ≤ 120 s. The deposition time ($t_{dep}$) was 60 min.

The plating bath contained 0.06 M $NiSO_4{\cdot}6H_2O$, 0.14 M $Na_2WO_4{\cdot}2H_2O$, 0.5 M $Na_3C_6H_5O_7{\cdot}2H_2O$, 0.5 M $NH_4Cl$, and 0.15 M NaBr (pH=9.5). A fresh plating bath was prepared for each experiment using chemical pure reagents and twice-distilled water. During the plating, the solution was gently stirred with a magnetic stirrer at 65 °C and degassed with purified nitrogen. Nickel coatings were obtained from the same bath, but in absence of the tungstate salt.

Deposit morphology was analyzed using an FEI, Quanta 200 scanning electron microscope (SEM). Surface composition was evaluated by X-ray photoelectron spectroscopy (XPS) using a Mg K$\alpha$ source (1,253.6 eV) from XR50, Specs GmbH and a hemispherical electron energy analyzer from PHOIBOS 100, Specs GmbH. Composition in depth was determined by argon ion sputtering (3 keV) at an average rate of 0.5–0.6 nm $min^{-1}$.

The electrochemical behavior of the Ni–W and Ni deposits and bulk Ni was studied with a Zahner IM6e potentiostat/galvanostat using a potentiodynamic linear polarization technique between preset cathodic ($E_{s,c}$) and anodic ($E_{s,a}$) switching potentials from the open circuit potential, at a potential scan rate ($v$) of $2\times10^{-3}$ V $s^{-1}$. A standard three-electrode cell was used. A large area Pt sheet counter electrode and a saturated calomel reference electrode (SCE) were used. All potentials in the text were referred to the SCE. Measurements were carried out in a still phosphate–borate buffer (0.1 M $KH_2PO_4$+0.05 M $Na_2B_4O_7$) pH8.00, with the addition of 1 M $Na_2SO_4$ at ambient temperature. Experiments were made under purified $N_2$ gas saturation.

The effect of oxygen on the open circuit potential ($E_{ocp}$) of the Ni–W alloys was evaluated after 1 h of immersion in the electrolyte. Corrosion current density values were obtained using the polarization resistance method [29] after 1 h and 24 h of immersion in the test solution.

## Results and discussion

XPS spectra were obtained to focus on the surface chemistry of the W–Ni alloy electrodeposited on carbon steel by different current pulse programs. Typical spectra for these alloys (τ = 120 s, $j$=70 mA $cm^{-2}$, $t_{dep}$=60 min) are shown in Fig. 1 before (a) and after (b) sputtering with $Ar^+$. The spectra show the presence of Ni, W, C, and O and the complete absence of Fe indicating that the Ni–W coating covers the carbon steel substrate completely. In fact, the thickness of these coatings is between 10 and 20 μm [11].

Data in Fig. 1 also show that the amount of C and O decreases while the Ni and W content markedly increases after sputtering the sample. The carbon 1s component at 283.4 eV (Fig. 1) suggests the presence of some tungsten carbide (WC) [11, 24, 30]. However, the presence of tungsten carbide could also result from implantation of carbon during the $Ar^+$ ion etching of the coating [26]. The presence of O is related to metal oxides on the coating surface. A similar behavior is observed for samples grown for τ values ranging from $5\times10^{-3}$ to 120 s.

A more detailed analysis of the Ni and W species in the electrodeposited alloy is shown in Fig. 2 where we plotted the Ni 2p and W 4f signals for different sputtering times. The high-resolution spectra reveal that the alloy surface ($t$=0 min) consists of a mixture of Ni oxides (NiO and NiOOH) and W oxide ($WO_3$). As the sputtering time increases, the amount of Ni and W oxides decreases while the metallic Ni and W content markedly increases. Note that the O content is reduced to a non-significant and constant level during the sputtering process. The metallic oxides are completely removed for $t$=45 min.

The XPS data in Table 1 show that the W/Ni ratio for the bulk alloy (sputtering time 45 min), $(W/Ni)_b$, remains nearly constant (≈0.3–0.4) irrespective of τ. In contrast, the XPS data for the alloy surface ($t$=0 min) reveal more differences in the oxide composition with the electrodeposition conditions (Fig. 3a–c). In fact, the XPS data show that the $WO_3$/W ratio at the surface, $(WO_3/W)_s$, decreases from ≈0.57 to 0.23 as $\tau$ is decreased. This is an important point since the electrochemical properties of the alloy are determined by its surface composition.

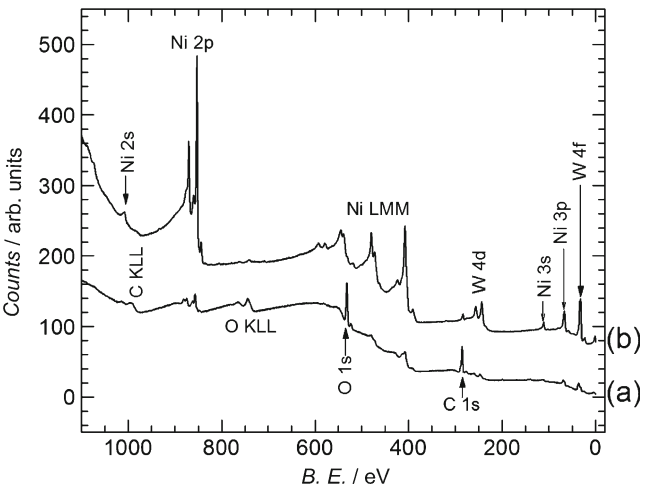


**Fig. 1** XPS spectra of a Ni–W alloy ($\tau$ = 120 s, $j$=70 mA $cm^{-2}$, $t_{dep}$= 60 min) taken at different etching times ($Ar^+$ bombardment), $t$: **a**) $t$= 0 min, **b**) $t$=45 min

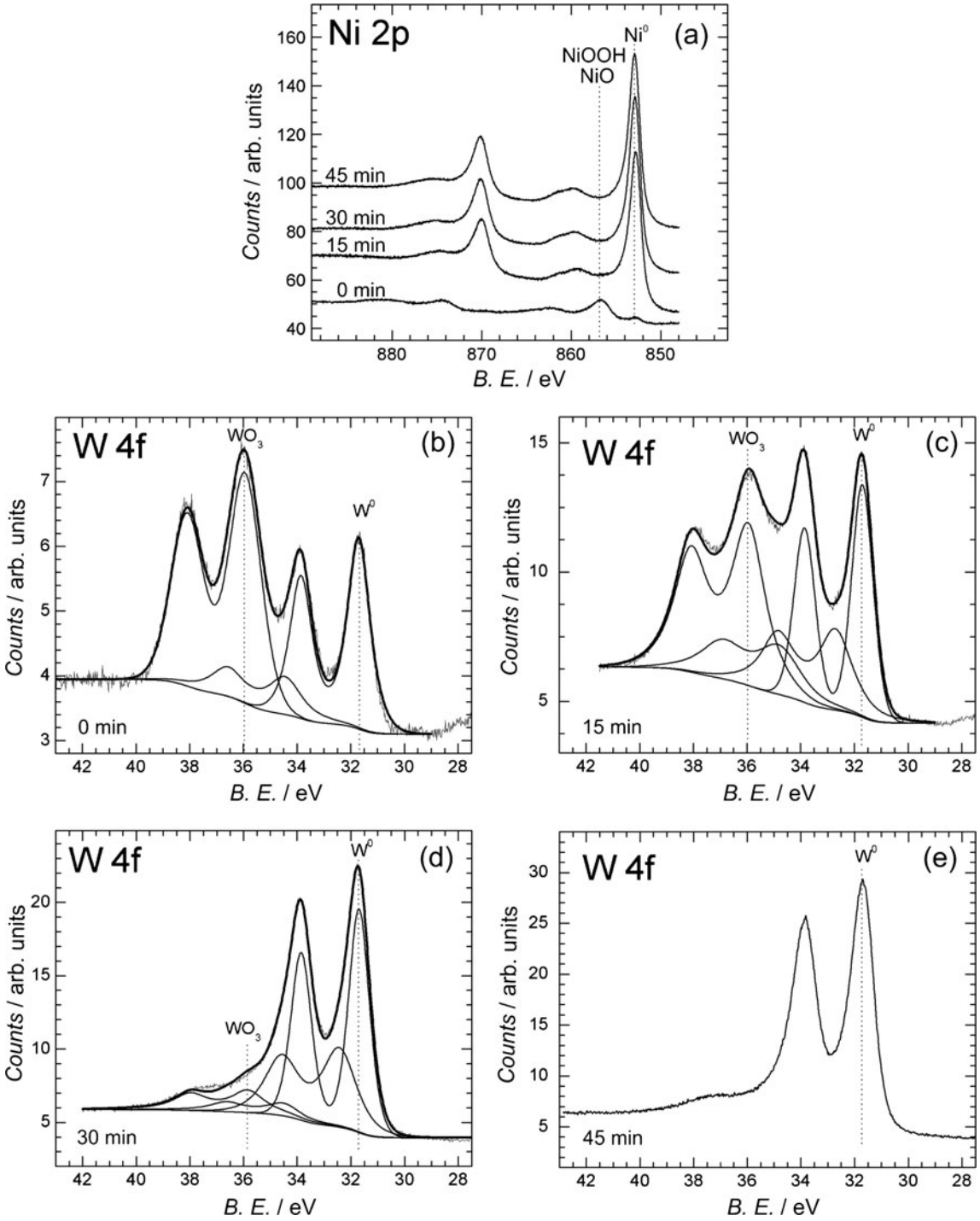


**Fig. 2** XPS spectra of a Ni–W alloy ($\tau$ =120 s, $j$=70 mA cm$^{-2}$, $t_{dep}$=60 min) taken at different sputtering times: **a**) Ni 2p, **b**–**e**) W 4f

The influence of τ on the surface structure of the Ni–W alloys may be inferred from the SEM images (Fig. 4) that reveal the presence of a fractal cauliflower-like structure formed by nanometer-sized units irrespective of τ. It means that the real surface area is too large with pores and channels interconnecting the structure.

Next, we present data about alloy electrochemical behavior to show its relation with surface chemistry and structure. Typical polarization curves for the Ni–W alloys recorded in the −0.7/0.5 V potential range and in the absence of $O_2$ are shown in Fig. 5. All the alloys exhibit the hydrogen evolution reaction (HER) in the cathodic branch and a limiting current in the anodic branch corresponding to the alloy dissolution ($j_{corr}$) through the complex passive film composed by NiO, NiOOH, and $WO_3$.

**Table 1** XPS data obtained corresponding to the bulk ($Ar^+$ bombardment, $t$=45 min) and surface ($t$ = 0) Ni–W alloy coatings electrodeposited at different $\tau$

| $\tau$ (s) | at.% $W_b$ | at.% $Ni_b$ | $(W/Ni)_b$ | $(WO_3/W)_s$ |
|---|---|---|---|---|
| $5\times10^{-3}$ | 22.7 | 77.3 | 0.3 | 0.23 |
| 10 | 30.0 | 70.0 | 0.41 | 0.57 |
| 120 | 29.0 | 71.0 | 0.40 | 0.56 |

HER on the Ni–W alloy is clearly enhanced in overpotentials ($\eta$) and current density ($j_H$) when compared with bulk Ni (Fig. 5a, b). In fact, the onset potential for HER on the Ni–W alloy surfaces is shifted to more positive potentials than that of bulk Ni. It can be argued that this enhancement could be produced by the presence of a certain amount of WC that is known to be an efficient HER catalyst [31]. However, our data show very similar $\eta$ values for HER on electrodeposited Ni samples and Ni–W alloys prepared under comparable conditions ($\tau=5\times10^{-3}$ s), thus discarding any possible effect of WC (Fig. 5a). This is not surprising as electrodeposited Ni is a nanostructured material and a clear

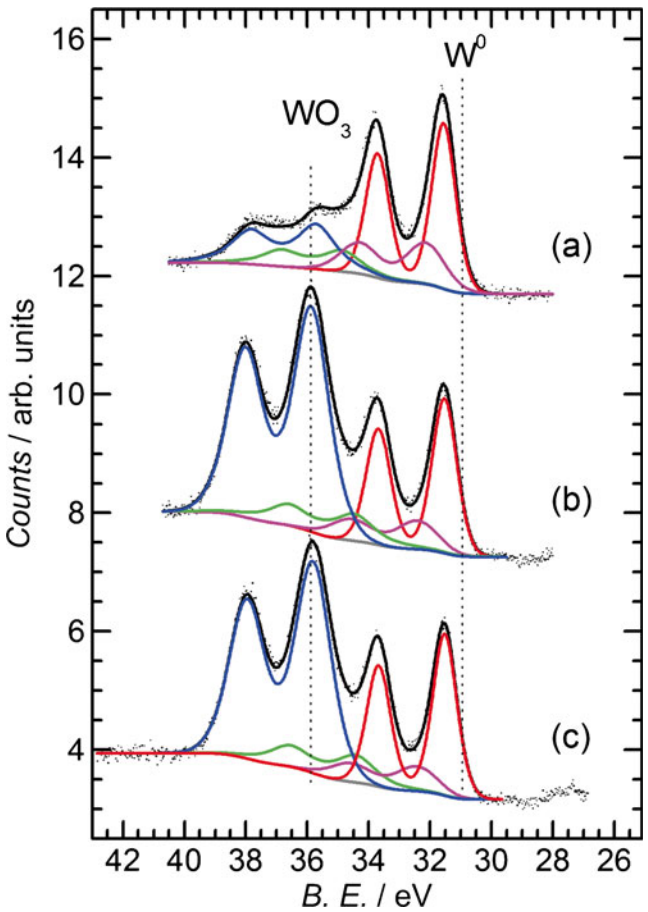


**Fig. 3** XPS W 4f spectra, at $t$=0 min ($Ar^+$ bombardment), of Ni–W alloys electrodeposited on carbon steel at different $\tau$: **a**) $5\times10^{-3}$ s, **b**) 10 s, **c**) 120 s

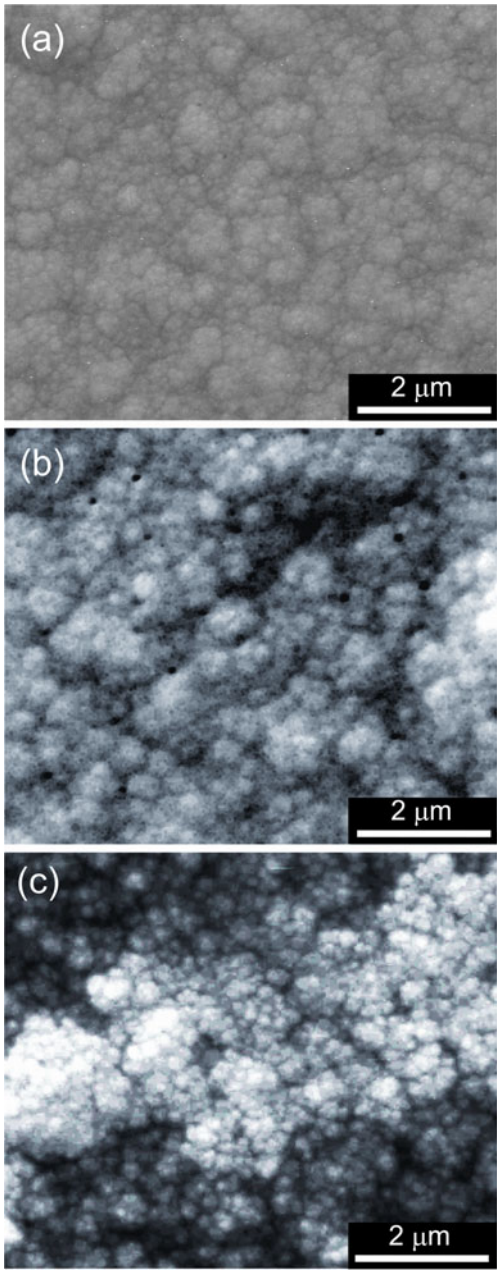


**Fig. 4** SEM micrographs of the surface of Ni–W deposits ($j$=70 mA $cm^{-2}$, $t_{dep}$=60 min) obtained at different $\tau$: **a**) $5\times10^{-3}$ s, **b**) 10 s, **c**) 120 s

increase in HER has been reported on this kind of Ni surfaces [32]. In fact, nanostructured materials exhibit different properties of their bulk phases due to the quantum effects related to the shape and size. Therefore, it can be concluded that the nanostructured cauliflower structure of the alloy surface contributes to HER enhancement.

We also observe lower $\eta$ values, and then a clear HER enhancement (Fig. 5c) on the Ni–W alloys surfaces richer in $WO_3$ ($\tau$=10 and 120 s, see Table 1). In relation to this subject, Savadogo et al. [33] have studied the HER using nickel electrodes with phosphotungstic acid. It has been

demonstrated that the presence of W in the form of $WO_3$ in the polyoxometalates enhanced the electrocatalytic activity for hydrogen evolution [33, 34]. Pt, when supported on tungsten trioxide, also showed electrocatalytic activity for HER due to the synergism towards reactions in an acid solution involving hydrogen atoms [35]. As previously shown, electrocatalytic activity changes markedly with the W/Ni ratio, being W/Ni=0.1 the best atomic ratio [36]. Our results, obtained from an almost constant W/Ni ratio (0.3/0.4) and similar surface structure, demonstrate that the $WO_3$ content at the surface is the key parameter controlling the HER electrocatalysis and reducing $\eta$ about 0.1 V (Fig. 5c).

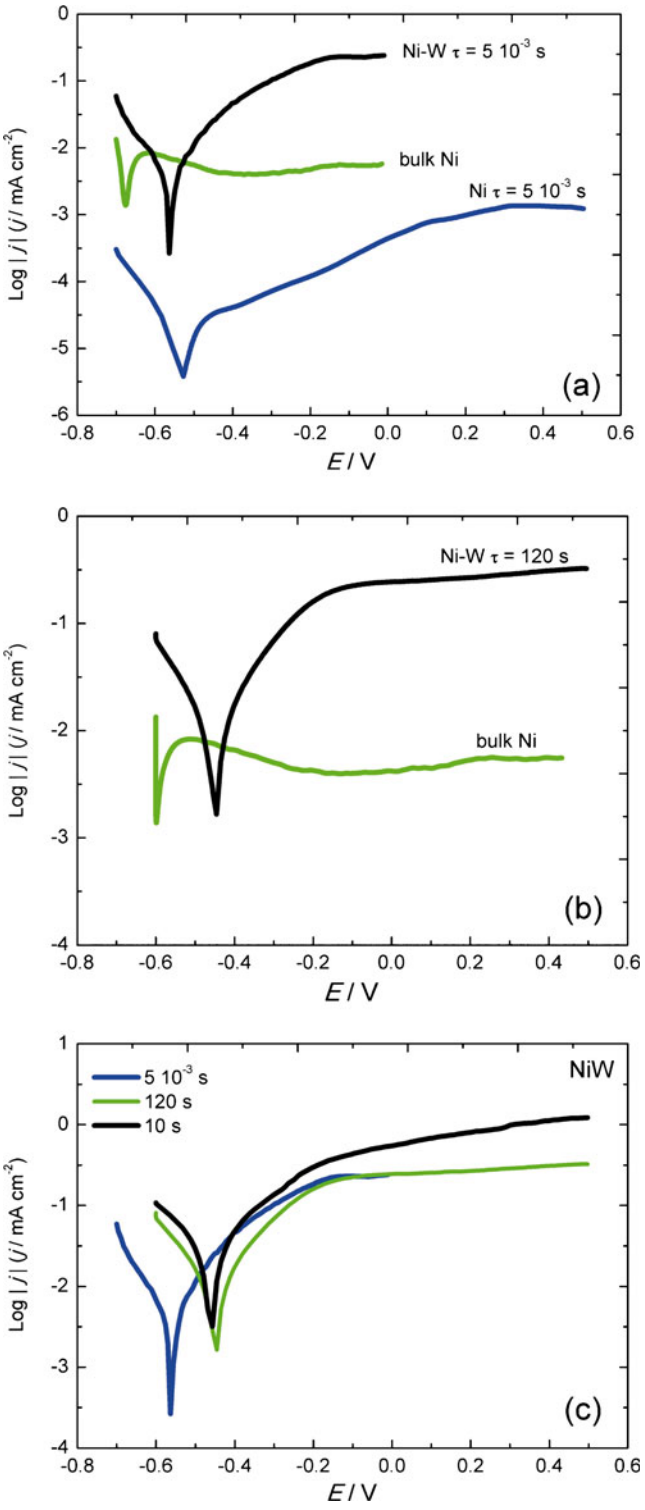


**Fig. 5** Polarization curves (log $j$ vs. $E$) obtained at $v=2\times10^{-3}$ V s$^{-1}$ in still phosphate–borate solution containing $Na_2SO_4$ 1 M: **a**) bulk Ni and electrodeposited Ni and Ni–W alloy obtained at $\tau=5\times10^{-3}$ s, **b**) bulk Ni and Ni–W alloy obtained at $\tau=120$ s, **c**) Ni–W alloys obtained at different $\tau$

**Table 2** Values of corrosion current densities ($j_{corr}$), using the polarization resistance method, obtained of Ni–W alloys electrodeposited at different $\tau$ after different exposure times in sulfate-containing electrolytes

| $\tau$ (s) | $j_{corr}$ (1 h) (μA cm$^{-2}$) | $j_{corr}$ (24 h) (μA cm$^{-2}$) |
|---|---|---|
| $5\times10^{-3}$ | 13.66 | 4.22 |
| 10 | 13.28 | 7.48 |
| 120 | 9.04 | 6.80 |

From the previous results, we can conclude that there are two aspects involved in the HER enhancement observed in the electrodeposited Ni–W alloys on steel: a nanostructured material and the chemical composition of the surface. They explain the catalytic activity on HER observed for $WO_3$ nanoparticles supported on C in acid and alkaline solutions [37].

However, coatings obtained at τ=120 s are fragile while those prepared at τ=10 s exhibit good mechanical properties [11]. Therefore, the best condition related to HER electrocatalysis and Ni–W mechanical properties is obtained at τ=10 s. A nanostructured alloy with the optimum $(WO_3/W)_s$ surface composition ratio is obtained in this condition.

When the anodic branch of polarization curves is analyzed (Fig. 5a, b), we observe that the nanostructured Ni–W alloys exhibit much larger dissolution current values than those of bulk Ni because of the presence of W and large

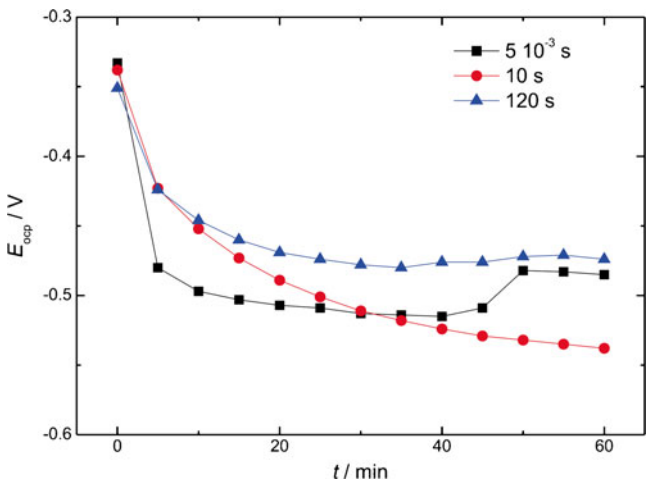


**Fig. 6** Open circuit potential evolution, $E_{ocp}$, of Ni–W alloys obtained at different $\tau$ in still phosphate–borate solution containing $Na_2SO_4$ 1 M

amounts of grain boundaries that make the film more defective. The tendency towards reaching a limiting current is due to the initial formation of protective NiO and NiOOH. This is in agreement with what was reported by other authors who demonstrated that at the same pH, Ni electrode passivity increases progressively as $E_{s,a}$ becomes more positive [38, 39]. In contrast, surface W and $WO_3$ tend to dissolve, giving tungstate ions [40–42] during the anodic potential sweep with the corresponding Ni oxide surface enrichment. Only at $E_{s,a}$ more positive than 0.2 V passivating tungsten oxides are known to be formed [41]. Other authors proposed other interpretations because they mainly used acid solutions containing chloride ions [4, 6, 8, 10–14, 21, 25]. Besides, few authors highlight the effect that the surface crystallographic condition exerts [13, 14].

The effect of oxygen in the open circuit potential value ($E_{ocp}$) of the alloys is shown in Fig. 6. The initial values lie in the potential windows where alloy dissolution takes place at $30<j_{corr}<100\ \mu A\,cm^{-2}$ as deduced from the polarization curves shown in Fig. 5c.

However, the dissolution rate is markedly reduced after 24-h immersion in the test solution as shown in Table 2. The largest change is observed in the deposits obtained at $\tau=5\times10^{-3}$ s since the $(WO_3/W)_s$ ratio is smaller than in those obtained at higher τ (Table 1). Hence, the enrichment and subsequent growth of Ni oxides is facilitated. The characteristic of the surface structure already shown and analyzed through SEM images (Fig. 4a) should be added.

Finally, even though the anodic branches of the polarization curves (Fig. 5a, b) indicate that bulk and electrodeposited Ni responses are better than those of the Ni–W deposits, the latter present larger values of hardness [5, 11], a valuable characteristic for technological applications.

From what has been analyzed above, we may infer that through the previous selected current pulse programs to obtain electrodeposited Ni–W alloys, we can handle the surface state (morphology and composition ratio among Ni, W, and their corresponding oxides), according to the desired application for the product since not any Ni–W coating, even if nanostructured, can be adequate to catalyze HER or to withstand corrosion in solutions containing aggressive ions.

These results are a good starting point to research the electrocatalytic activity for HER that these nanostructured Ni–W alloys present in NaOH solutions to simulate industrial electrolysis conditions and to evaluate corrosion resistance in solutions containing other aggressive anions (sulfide and chloride).

## Conclusions

Ni–W alloys electrodeposited on carbon steel by different current pulse programs were obtained.

All the Ni–W alloy surfaces exhibited a fractal cauliflower-like structure irrespective of τ. It means that the surface has a large real surface area approaching a volume with a large number of pores and channels. However, the coatings obtained at low frequencies showed brittleness.

The surface composition ratio, $(WO_3/W)_s$, of the Ni–W electrodeposits defines if the alloys may act as HER catalyzers or be corrosion resistant in neutral media containing sulfate ions. It was possible to demonstrate that the Ni–W nanostructured coating, with a large effective area, lack of fragility, and higher $(WO_3/W)_s$ ratio, offers an optimal condition to work as a stable electrode to catalyze HER, thus exceeding the catalytic activity that bulk and electrodeposited Ni have.

To improve the corrosion resistance in neutral media containing sulfate anions, a lower $(WO_3/W)_s$ ratio is needed so that Ni and its oxides may provide protection. This situation is obtained for coatings obtained at low τ.

**Acknowledgments** We acknowledge financial support from the Consejo Nacional de Investigaciones Científicas y Técnicas (CONICET, PIP 03079), the Agencia Nacional para la Promoción de la Ciencia y la Tecnología Argentina (ANPCyT, PICT 2010-2554, PICT CNPQ-0019), and Consejo de Investigaciones de la Universidad Nacional de Tucumán, Argentina. MEV is member of the research career of CICPBA, Argentina.

## References

1. Yamasaki T (2000) Mater Phys Mech 1:127–132
2. Younes O, Zhu L, Rosenberg Y, Shacham-Diamond Y, Gileadi E (2001) Langmuir 17:8270–8275
3. Cesiulis H, Baltutiene A, Donten M, Donten ML, Stojek Z (2002) J Solid State Electrochem 6:237–244
4. Yang F-Z, Guo Y-F, Huang L, Xu S-K, Zhou S-M (2004) Chin J Chem 22:228–231
5. Sriraman KR, Ganesh Sundara Raman S, Seshadri SK (2006) Mater Sci Eng A 418:303–311
6. Sriraman KR, Ganesh Sundara Raman S, Seshadri SK (2007) Mater Sci Eng A 460–461:39–45
7. Detor AJ, Schuh CA (2007) Acta Mater 55:371–379
8. Alimadadi H, Ahmadi M, Aliofkhazraei M, Younesi SR (2009) Mater Des 30:1356–1361
9. Cardinal MF, Castro PA, Baxi J, Liang H, Williams FJ (2009) Surf Coat Technol 204:85–90
10. de Lima-Neto P, Correia AN, Santana RAC, Colares RP, Barros EB, Casciano PNS, Vaz GL (2010) Electrochim Acta 55:2078–2086
11. Quiroga Argañaraz MP, Ribotta SB, Folquer ME, Gassa LM, Benítez G, Vela ME, Salvarezza RC (2011) Electrochim Acta 56:5898–5903
12. Zemanová M, Krivosudská M, Chovancová M (2011) J Appl Electrochem 41:1077–1085
13. Chianpairot A, Lothongkum G, Schuh CA, Boonyongmaneerat Y (2011) Corros Sci 53:1066–1071
14. Farzaneh MA, Zamanzad-Ghavidel MR, Raeissi K, Golozar MA, Saatchi A, Kabi S (2011) Appl Surf Sci 257:5919–5926
15. Obradović MD, Stevanović J, Stevanović RM, Despić AR (2000) J Electroanal Chem 491:188–196

16. Younes O, Gileadi E (2002) J Electrochem Soc 149(2):C100–C111
17. Younes-Metzler O, Zhu L, Gileadi E (2003) Electrochim Acta 48:2551–2562
18. Obradović MD, Bošnjakov GŽ, Stevanović RM, Maksimović MD, Despić AR (2006) Surf Coat Technol 200:4201–4207
19. Zhu L, Younes O, Ashkenasy N, Shacham-Diamond Y, Gileadi E (2002) Appl Surf Sci 200:1–14
20. Yamasaki T, Schloβmacher P, Ehrlich K, Ogino Y (1998) Nanostruct Mater 10:375–388
21. Krolikowski A, Plonska E, Ostrowski A, Donten M, Stojek Z (2009) J Solid State Electrochem 13:263–275
22. Donten M, Cesiulis H, Stojek Z (2000) Electrochim Acta 45:3389–3396
23. Younes O, Gileadi E (2000) Electrochem Solid State Lett 3:543–545
24. Obradović M, Stevanović J, Despić A, Stevanović R, Stoch J (2001) J Serb Chem Soc 66(11–12):899–912
25. Sassi W, Dhouibi L, Berçot P, Rezrazi M, Triki E (2012) Surf Coat Technol 206:4235–4241
26. Quiroga Argañaraz MP, Ribotta SB, Folquer ME, Zelaya E, Llorente C, Ramallo-López JM, Benítez G, Rubert A, Gassa LM, Vela ME, Salvarezza RC (2012) Electrochim Acta 72:87–93
27. Lucente AM, Scully JR (2007) Corros Sci 49:2351–2361
28. Acosta CC, Salvarezza RC, Videla HA, Arvia AJ (1985) Corros Sci 25:291–303
29. Jones DA (1992) Principles and prevention of corrosion. Macmillan, New York
30. Juškėnas R, Valsiūnas I, Pakštas V, Giraitis R (2009) Electrochim Acta 54:2616–2620
31. Harnisch F, Sievers G, Schröder U (2009) Appl Catal B Environ 89:455–458
32. Lin S-C, Chiu Y-F, Wu P-W, Hsieh Y-F, Wu C-Y (2010) J Mater Res 25:2001–2007
33. Savadogo O, Ndzebet E (1993) J Appl Electrochem 23:915–921
34. Savadogo O (1993) Mater Chem Phys 35:145–150
35. Abbaro SA, Tseung ACC, Hibbert DB (1980) J Electrochem Soc 127:1106–1107
36. Metikoš-Huković M, Grubač Z, Radić N, Tonejc A (2006) J Mol Catal Chem 249:172–180
37. Zheng H, Mathe M (2011) Int J Hydrogen Energy 36:1960–1964
38. Gassa LM, Vilche JR, Arvia AJ (1983) J Appl Electrochem 13:135–145
39. Barral G, Njanjo-Eyoke F, Maximovitch S (1995) Electrochim Acta 40:709–718
40. Ortiz PI, López Teijelo M, Giordano MC (1988) J Electroanal Chem 243:379–391
41. Anik M, Osseo-Asare K (2002) J Electrochem Soc 149:B224–B233
42. Anik M (2010) Corros Sci 52:3109–3117